scientific reports

Check for updates

OPEN

Cytoplasmic HIF-2α as tissue biomarker to identify metastatic sympathetic paraganglioma

Sinan Karakaya[1,2,3,11], Lisa Gunnesson[4,5,11], Erik Elias[4,5], Paula Martos-Salvo[1,2,3], Mercedes Robledo[6], Ola Nilsson[7], Bo Wängberg[4,5], Frida Abel[8,9], Sven Påhlman[3,10], Andreas Muth[4,5,12] & Sofie Mohlin[1,2,3,12]✉

Pheochromocytomas (PCCs) and paragangliomas (PGLs) are rare neuroendocrine tumors. PGLs can further be divided into sympathetic (sPGLs) and head-and-neck (HN-PGLs). There are virtually no treatment options, and no cure, for metastatic PCCs and PGLs (PPGLs). Here, we composed a tissue microarray (TMA) consisting of 149 PPGLs, reflecting clinical features, presenting as a useful resource. Mutations in the pseudohypoxic marker HIF-2α correlate to an aggressive tumor phenotype. We show that HIF-2α localized to the cytoplasm in PPGLs. This subcompartmentalized protein expression differed between tumor subtypes, and strongly correlated to proliferation. Half of all sPGLs were metastatic at time of diagnosis. Cytoplasmic HIF-2α was strongly expressed in metastatic sPGLs and predicted poor outcome in this subgroup. We propose that higher cytoplasmic HIF-2α expression could serve as a useful clinical marker to differentiate paragangliomas from pheochromocytomas, and may help predict outcome in sPGL patients.

Pheochromocytomas (PCCs) and paragangliomas (PGLs) are rare neuroendocrine tumors originating from neural crest-derived schwann cell precursors in the adrenal medulla, sympathetic ganglionic tissue in the abdomen or thorax, or parasympathetic ganglionic tissue mainly in the head- and neck region[1,2].

Radical surgery is curative in most patients. Still, while most tumors display a non-metastatic phenotype, around 10% of pheochromocytomas and paragangliomas (PPGLs) develop metastases[3]. There are no reliable markers to conclusively demonstrate malignant potential of primary tumors. The 2017 WHO classification[4] adopted the position that all PPGLs have malignant potential and instead made a distinction between non-metastatic and metastatic tumors. Since limited treatment options exist for patients with metastatic PPGL, better prognostic and predictive markers are needed for tailored treatment and follow-up.

PPGLs have the highest rate of heritability of all human solid tumors with up to 40% carrying germline mutations. The majority of familial PPGL tumors are caused by pathogenic variants in one of the four Succinate dehydrogenase subunit genes (*SDH*x). Sporadic PPGL harbor somatic driver mutations in some of the same genes as inherited predisposition syndromes (*e.g., RET*, *VHL*, *NF1*, *SDHB*), as well as in additional genes (*e.g., HRAS*, *EPAS1*)[5–9].

Overall, there are over 20 susceptibility genes identified in PPGL[10], and tumors can be divided into three broad groups; the pseudohypoxic cluster 1 with mutations in *VHL*, *SDH*x, *EGLN1/PHD2*, *FH* and *EPAS1* genes[11], the kinase signaling cluster 2 with mutations in *RET*, *NF1*, *HRAS*, *MAX*, *TMEM127*, and the wnt pathway cluster 3 with *MAML3* fusions and mutations in *CSDE1*[7]. Mutations in the first group lead to increased stabilization of hypoxia inducible factor (HIF)-2α and a metabolic switch into a persistent pseudohypoxic state (*i.e.,* hypoxic

[1]Division of Pediatrics, Department of Clinical Sciences, Lund University, Sölvegatan 19, BMC B11, 223 84 Lund, Sweden. [2]Lund Stem Cell Center, Lund University, Lund, Sweden. [3]Lund University Cancer Center, Lund University, Lund, Sweden. [4]Department of Surgery, Sahlgrenska University Hospital, Gothenburg, Sweden. [5]Department of Surgery, Institute of Clinical Sciences, Sahlgrenska Academy, University of Gothenburg, Gothenburg, Sweden. [6]Hereditary Endocrine Cancer Group, Spanish National Cancer Research Centre (CNIO), 28029 Madrid, Spain. [7]Department of Laboratory Medicine, Institute of Biomedicine, Sahlgrenska Academy, University of Gothenburg, Gothenburg, Sweden. [8]Department of Clinical Genetics and Genomics, Sahlgrenska University Hospital, Gothenburg, Sweden. [9] Department of Laboratory Medicine, Institute of Biomedicine, Sahlgrenska Academy, Gothenburg University, Gothenburg, Sweden. [10]Translational Cancer Research, Department of Laboratory Medicine, Lund University, Lund, Sweden. [11]These authors contributed equally: Sinan Karakaya and Lisa Gunnesson. [12]These authors jointly supervised this work: Andreas Muth and Sofie Mohlin. ✉email: sofie.mohlin@med.lu.se

phenotype in oxygenated conditions), while mutations in the kinase signaling group of genes activate the PI3K/AKT/mTOR and RAS/RAF pathways[12,13].

Oxygen sensing is one of the most important evolutionary traits of multicellular organisms (reviewed in Hammarlund et al.[14]). During physiological settings when oxygen is present, HIFs are targeted for degradation. There are however mechanisms by which HIFs escape this, *e.g.,* loss-of-function mutations in the genes encoding VHL or PHD, generating pseudohypoxic phenotypes. While both HIF-1α and HIF-2α respond to oxygen fluctuations, it is primarily HIF-2α that has been implicated in tumor progression. For example, the majority of clear cell renal cell carcinomas are driven by mutations in *VHL*, leading to complete HIF-2-driven tumor formation[15].

Ten years ago, the first mutation in *EPAS1* (encoding HIF-2α) in cancer was detected[16]. Two novel mutations were found in PGL patients, associated with increased protein half-life and HIF-2α activity[16]. Since then, a number of *EPAS1* mutations have been detected in PPGL[17–23]. Fliedner et al. further defined *EPAS1* mutated tumors as a subcluster of the pseudohypoxic cluster 1 PGLs, separated from other hereditary pseudohypoxic PGLs driven by *VHL* or *SDHx* genes[24]. Recently, mutations in *EPAS1* have been detected also in esophageal squamous cell carcinoma and colorectal cancer[25,26].

HIF-2α acts as a nuclear transcription factor. However, emerging evidence show that HIF-2α can localize to the cytoplasm in neuroblastoma[27,28] and glioblastoma[29]. In similarity to PPGL, neuroblastoma arises along the sympathetic ganglia and in adrenal glands, and originates from stem cells of the neural crest. We recently showed that HIF-2α is expressed in the cytoplasm of migrating neural crest cells[30], demonstrating the importance of understanding HIF-2α expression and biology in PPGL.

We provide here a comprehensive PPGL TMA with an in-depth characterization of the material. All sympathetic paragangliomas (sPGL) specimens were positive for cytoplasmic HIF-2α and more than half of these patients presented with metastasis at time of diagnosis. Staining of Ki-67 as a proxy for proliferation is an important clinical parameter. We found that cytoplasmic HIF-2α strongly correlated with Ki-67, and high expression of cytoplasmic HIF-2α predicted poor outcome in sPGLs. Our results utilizing this TMA for biological analyses suggest that the cytoplasmic fraction of the HIF-2α protein separates metastatic from non-metastatic sPGLs, confers aggressive features, and predicts outcome. We propose further studies to establish and implement cytoplasmic HIF-2α expression as a clinical marker for poor outcome in sPGL.

Material and methods

Clinical material. A total of 149 patients diagnosed with PPGL at Sahlgrenska University Hospital, Gothenburg, Sweden, between 1984 and 2015 were included in the TMA. The study was approved by the local ethical board of Gothenburg and all methods performed were in accordance with the guidelines and regulations of the local ethical board of Gothenburg (ethical permit no. 833-18). The informed consent has been obtained from each patient or subject after full explanation of the purpose and nature of all procedures used. Patient information concerning age, sex, recurrent or metastatic disease as well as hormone profile of the tumors and causes of death when applicable was retrieved from in-patient charts and a pre-existing clinical database. Clinical pathology reports were searched for any further tumor specific data. Characterization of the material is summarized in Table 1.

Tissue microarray and immunohistochemical staining. PPGL patient material was retrieved from the pathology archives at Sahlgrenska University Hospital, Gothenburg. Tumor cores were formalin-fixed and paraffin-embedded into TMA blocks. From representative tumor areas selected by a board-certified pathologist (O.N.), tissue core biopsies were punched out and mounted in recipient blocks. A total of 175 donor tumor cores with 149 unique primary tumors were included in the TMA. Sufficient core quality was assessed by eosin staining. Sections (4 µm) were stained using AutostainerPlus (Dako). The TMA was stained for chromogranin A (CgA, MAB319, Merck Millipore 1:4000), synaptophysin (SYP, M0776, Agilent, 1:200 + Linker), tyrosine hydroxylase (TH, ab75875, Abcam, 1:300), vimentin (ab45939, Abcam, 1:200), HIF-1α (610959, BD Biosciences, 1:50 + Linker), HIF-2α (A700-003, Bethyl Labs, 1:200 + Linker; AB207607, Abcam, 1.50 + Linker), DEC1/BHLHE40 (nb100-1800, Novus Biologicals, 1:100), SDHB (459230, Invitrogen, 1:250), and Ki-67 (IR62661, Agilent, Ready-to-use + Linker). The slides were digitalized with Axio Scan Z.1 at 20 × magnification.

TMA staining of HIF-2α. Formalin-fixed paraffin-embedded PPGL patient TMA tissue cores were sectioned at 4 µm and prepared for further analysis. TMA slides were deparaffinised and rehydrated by incubation three times in Xylene, twice in 100% ethanol, twice in 96% ethanol, and twice in 70% ethanol for three minutes in each solution respectively, and rinsed with ddH_2O. Slides were then incubated in pH 9 (TRIS–EDTA based) antigen retrieval buffer at 97 °C for 20 min in an Agilent PT-Link instrument. After the slides had cooled down for 30 min, slides were stained for HIF-2α using Agilent EnVision FLEX, High pH (Link) kit as well as Dako Cytomotion Autostainer. During the procedure, slides were incubated with EnVision FLEX Peroxidase-Blocking Reagent for 5 min to block endogenous peroxidases. Slides were incubated with HIF-2α antibody (A700-003, Bethyl Labs) diluted 1:200 in EnVision FLEX Antibody Diluent for 30 min at room temperature. Slides were then incubated with EnVision FLEX + Rabbit (LINKER) for 15 min for signal amplification, and treated with EnVision FLEX/HRP visualization reagent for 20 min. This was followed by incubation with EnVision FLEX DAB + Chromogen diluted in EnVision FLEX Substrate Buffer. In the last step, counterstaining was performed by incubating the slides in EnVision FLEX Hematoxylin for three minutes. Slides were finally mounted using organic solvent-based mounting medium. Between all steps, slides were washed with EnVision FLEX Wash Buffer. Antibody specificity was confirmed by staining hypoxic (1% oxygen) and normoxic (21% oxygen) SK-N-BE(2)c neuroblastoma, and VHL negative renal cell carcinoma 786-O and RCC-4 cells (Supplementary Fig. S1).

	sPGL (%)		HN-PGL (%)		PCC (%)		PPGL (%)		
Gender	Female (%)	Male (%)	Female (%)	Male (%)	Female (%)	Male (%)	Female (%)		Male (%)
	6 (46)	7 (54)	6 (46)	7 (54)	68 (55)	55 (45)	80 (54)		69 (46)
Age of diagnosis	Mean age (range)		Mean age (range)		Mean age (range)		Median age (range)		
	54 (32–72)		47 (22–76)		51 (15–83)		53 (15–83)		
Diagnosis	13 (9)		13 (9)		123 (82)		149 (100)		
Metastatic status	Non-metastatic (%)	Metastatic (%)	Non-metastatic (%)	Metastatic (%)	Non-metastatic (%)	Metastatic (%)	Non-metastatic (%)		Metastatic (%)
	7 (54)	6 (46)	13 (100)	0 (0)	118 (96)	5 (4)	138 (93)		11 (7)
Tumour location	Non-metastatic (%)	Metastatic (%)	Non-metastatic (%)	Metastatic (%)	Non-metastatic (%)	Metastatic (%)	Non-metastatic (%)		Metastatic (%)
Adrenal gland	–	–	–	–	118 (96)	5 (4)	118 (79)		5 (2)
Head and neck	–	–	13 (100)	0 (0)	–	–	13 (9)		0 (0)
Thorax or abdomen	7 (54)	6 (46)	–	–	–	–	7 (5)		6 (5)
Biochemical phenotype	Non-metastatic (%)	Metastatic (%)	Non-metastatic (%)	Metastatic (%)	Non-metastatic (%)	Metastatic (%)	Non-metastatic (%)	Metastatic (%)	Total (%)
Unknown	3 (100)	0 (0)	–	–	15 (94)	1 (6)	18 (95)	1 (5)	19 (100)
Biochemically silent	2 (20)	3 (30)	13 (100)	0 (0)	3 (3)	0 (0)	18 (14)	3 (2)	21 (16)
Hormone secreting	2 (20)	3 (30)	–	–	100 (93)	4 (4)	102 (78)	7 (5)	109 (84)
Adrenergic	–	–	–	–	63 (59)	1 (1)	63 (48)	1 (1)	64 (49)
Noradrenergic	2 (20)	3 (30)	–	–	36 (33)	2 (2)	38 (29)	5 (3)	43 (33)
Dopaminergic	–	–	–	–	1 (1)	1 (1)	1 (1)	1 (1)	1 (2)
Mutation/diagnosis	Non-metastatic (%)	Metastatic (%)	Non-metastatic (%)	Metastatic (%)	Non-metastatic (%)	Metastatic (%)	Non-metastatic (%)	Metastatic (%)	Total (%)
Unknown	1 (33)	2 (67)	9 (100)	0 (0)	36 (100)	0 (0)	46 (96)	2 (4)	48 (100)
No mutation	4 (40)	0 (0)	–	–	47 (54)	3 (4)	51 (51)	3 (3)	54 (54)
Somatic or germline mutations	2 (20)	4 (40)	4 (100)	0 (0)	35 (40)	2 (2)	41 (40)	6 (6)	47 (46)
SDHx	1 (10)	4 (40)	4 (100)	0 (0)	2 (2)	2 (2)	7 (6)	6 (6)	13 (12)
EPAS1	1 (10)	0 (0)	–	–	–	–	1 (1)	0 (0)	1 (1)
RET	–	–	–	–	17 (20)	0 (0)	17 (17)	0 (0)	17 (17)
VHL	–	–	–	–	6 (7)	0 (0)	6 (6)	0 (0)	6 (6)
HRAS	–	–	–	–	2 (2)	0 (0)	2 (2)	0 (0)	2 (2)
NF1	–	–	–	–	8 (9)	0 (0)	8 (8)	0 (0)	8 (8)

Table 1. General characteristics of the patient cohort.

To confirm cytoplasmic HIF-2α expression in PPGL, we also conducted immunofluorescent staining with PPGL cell line, hPheo1, using two different antibodies against HIF-2α (Supplementary Fig. S2).

TMA scoring. Immunohistochemical (IHC) staining was viewed and examined blindly by two independent persons using the PathXL software. A second independent assessment was conducted by an independent person using QuPath-0.3.0 software[31]. The software's TMA dearrayer was applied to each slide to detect individual tumor cores and manually corrected when necessary. For CgA, SYP, TH, VIM and HIF-2α-C a scoring intensity of negative (0), weak (1 +), median (2 +) and strong (3 +) tumor cell specific expression was manually determined (representative images in Supplementary Fig. S3). Additionally, H-Score between 0 and 300 was calculated for HIF-2α-C staining for each tumor core by using QuPath-0.3.0 software. For this, cell detection command was used to identify each cell based on nuclear hematoxylin staining in every tumor core, then, intensity thresholds were set to distinguish cells with negative, weak, intermediate, and strong cytoplasmic HIF-2α based on DAB staining. The cores having H-Score between 0 and 15 scored as negative (0), 16–99 scored as weak (1 +), 100–199 scored as intermediate (2 +) and 200–300 scored as strong (3 +). Four *EPAS1* mutated tumors (1 PCC, 3 sPGL, all non-metastatic) from the CNIO cohort[32] were stained for HIF-2α using the same protocol as above. Scoring was performed by an independent person using the QuPath-0.3.0 software as described above. For HIF-1α, DEC1/BHLHE40 and nuclear HIF-2α staining, tumor cell specific expression scoring was determined semi-automatically by using QuPath-0.3.0 software. Each TMA core and cells were detected as above and then tumor cells with nuclear DAB staining were manually counted. The tumor cores with positive cancer cell percentages between 0 and 1% scored as negative (0), 1–5% scored as weak (1 +), 5–10% scored as intermediate (2 +) and > 10% scored as strong (3 +). For the Ki-67 staining, the number of positive and negative cells in the hotspot regions detected by a pathologist was manually counted and percentage of positive cells were calculated for each tumor core. The tumor cores with positive cancer cell percentages between 0% scored as negative (0), 0–1% scored as weak (1 +),

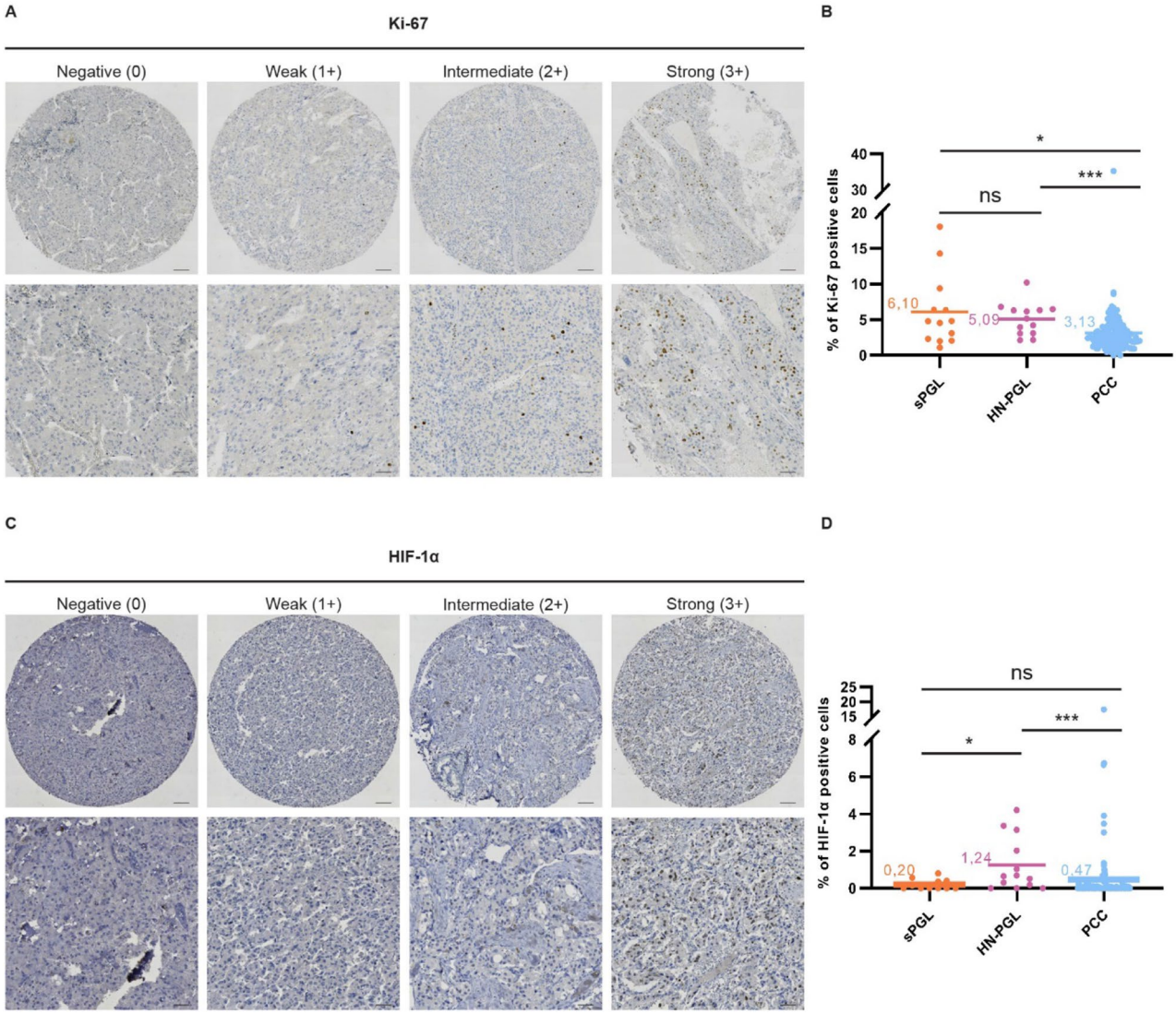

Figure 1. PPGLs express low levels of Ki-67 and HIF-1α. (**A**) Representative images from tumor cores scored as negative (0), weak (1+), intermediate (2+) or strong (3+) for Ki67. (**B**) Quantification of Ki67 positive cells (in %). (**C**) Representative images from tumor cores scored as negative (0), weak (1+), intermediate (2+) or strong (3+) for HIF-1α. (**D**) Quantification of HIF-1α positive cells (in %). Tumor cores were scored manually by three independent researchers as well as semi-automatically using the QuPath-0.3.0 software. Statistical significance was determined by the Mann–Whitney test. sPGL, sympathetic paraganglioma; HN-PGL, head- and neck paraganglioma; PCC, pheochromocytoma. The scale bar represents 100 µm in core images and 50 µm in zoomed images.

1–3% scored as intermediate (2+) and > 3% scored as strong (3+) (Kimura et al. 2018). Cells of necrosis, healthy tissue, scanning and staining artifacts and folded areas were manually removed from the calculation. Coherence between manual and semi-automated scoring by QuPath-0.3.0 software was analyzed for a fraction of markers by Kappa score. We could confirm a good agreement between the two ways of scoring (Supplementary Table S1).

Genetics. Germline mutational data of *SDHA*, *SDHB*, *SDHC*, *SDHD*, *RET*, *VHL*, and *NF1* were collected from the two clinical genetics laboratories and oncogenetic clinics at the University hospitals in Gothenburg and Lund (Supplementary Table S2). Genetic screening of the proband/affected family member was performed using Sanger DNA sequencing or massive parallel sequencing panels, and for patients diagnosed from 2014 and onwards the analyses were combined with multiplex ligation-dependent probe amplification (MLPA, P081-D1 & P082-C2 (NF1), P226-D1 (SDHx), and P016-C2 (VHL), MRC-Holland, Amsterdam, The Netherlands) for the detection of large deletions or duplications. Whole exome sequencing (WES) data from 23 PPGL cases was extracted from previous published papers[10,33]. WES was run as either paired tumor tissue and normal tissue/blood (10 cases) or as single tumor tissue (13 cases), and identified additional germline and somatic variants in PPGL susceptibility genes (i.e., *NF1*, *VHL*, *RET*, *EPAS1* and *HRAS*). Tumor samples with no apparent causative point mutation were further analyzed for exon/gene deletions or duplications by MLPA as described above.

Marker	Diagnosis/intensity	Negative (%)	Weak (%)	Intermediate (%)	Strong (%)	Positive (%)	# of Tumors (%)
Ki-67	*sPGL*	0 (0)	0 (0)	4 (31)	9 (69)	13 (100)	13 (100)
	HN-PGL	0 (0)	0 (0)	2 (16)	11 (84)	13 (100)	13 (100)
	PCC	2 (2)	13 (10)	59 (48)	49 (40)	121 (98)	123 (100)
HIF-1α	*sPGL*	11 (100)	0 (0)	0 (0)	0 (0)	0 (0)	11 (100)
	HN-PGL	8 (62)	5 (38)	0 (0)	0 (0)	5 (38)	13 (100)
	PCC	106 (91)	7 (6)	1 (1)	3 (2)	11 (9)	117 (100)
HIF-2α-N	*sPGL*	8 (61)	4 (31)	1 (8)	0 (0)	5 (39)	13 (100)
	HN-PGL	1 (8)	7 (58)	1 (8)	3 (26)	11 (92)	12 (100)
	PCC	97 (82)	20 (16)	2 (2)	0 (0)	22 (18)	119 (100)
HIF-2α-C	*sPGL*	0 (0)	4 (31)	7 (54)	2 (15)	13 (100)	13 (100)
	HN-PGL	0 (0)	1 (8)	5 (42)	6 (50)	12 (100)	12 (100)
	PCC	15 (13)	65 (54)	33 (28)	6 (5)	104 (87)	119 (100)

Table 2. Staining characteristics of the patient cohort.

Only variants predicted to be pathogenic or likely pathogenic by the American College of Medical Genetics and Genomics[34] were included in the final mutation list (Table 1)[34]. All tumor cores were stained for SDHB to determine *SDHx* loss-of-function for patients with unknown mutational status. Samples with negative SDHB staining were included in the list of patients with known mutations, designated as SDHx mutated (Table 1 and Supplementary Table S2).

mRNA expression analyses. For 23 PPGL samples analyzed in the current study, mRNA expression data from fresh tumor tissue run by 44 K Agilent Cy3/Cy5 2-color microarrays (Agilent) were available. Tumor samples were divided into expression groups based on previous unsupervised hierarchical clustering using a 153 discriminative gene set[33]. Normalized and log transformed expression data from different PPGL data sets (TCGA, (E-MTAB-733)[35], (GSE67066)[36]) were downloaded from 'R2: Genomics Analysis and Visualization Platform' (http://r2.amc.nl).

Statistics. GraphPad Prism 9 software was used for correlation, statistical and survival analyses. Mann–Whitney test was used to determine statistical significance. Fisher's exact test was used to determine the statistical difference in nuclear and cytoplasmic HIF-2α expression between patients diagnosed with sPGL, HN-PGL and PCC. p-value was employed as; $p < 0.05$ (*), $p < 0.01$(**), $p < 0.001$(***) and $p < 0.0001$(****) if not otherwise specified. Spearman's correlation test was used to calculate the correlation coefficient and statistical significance (two-tailed P value for each correlation coefficient). Kaplan–Meier survival analysis and the Log-rank (Mantel–Cox) test were used to prepare and compare survival curves, respectively.

Results

Characterization of patient material. The TMA was constructed from donor blocks of 175 fixed primary, recurrent and metastatic tumor tissue from 149 patients diagnosed and operated for PPGL at Sahlgrenska University Hospital, Gothenburg, Sweden, between 1983 and 2015. After removal of recurrent, metastatic, and duplicate cores, 149 primary tumor cores obtained from individual patients were used in the analyses. The patient material (Table 1) is coherent with previously published population-based data[37]. The majority of patients were diagnosed with PCCs (n = 123), while the rest were diagnosed with PGLs (n = 26; 13 sPGLs and 13 head- and neck (HN)-PGLs). At time of diagnosis, 93% (n = 138) of the tumors were considered non-metastatic while 7% (n = 11) were diagnosed as metastatic. A substantially higher proportion of sPGLs were considered metastatic as compared to PCCs (46% vs. 4% respectively). None of the thirteen HN-PGLs were metastatic at time of diagnosis, in line with an overall low malignancy rate among these tumors[38]. In total, 47 patients (46%) were found to have somatic, or germline mutations known to be associated with PPGL (Table 1), in coherence with previous data[39,40].

sPGLs are more proliferative than PCCs. We stained our TMA for diagnostic PPGL markers Chromogranin A (CgA), tyrosine hydroxylase (TH), vimentin (VIM), and synaptophysin (SYP) (Supplementary Fig. S3). All proteins were expressed as expected (Supplementary Fig. S3 and Supplementary Table S3). None of these markers differentiated non-metastatic vs. metastatic PPGLs (Supplementary Table S4). Generally, PPGLs are slow growing tumors with low proliferation rates, and Ki-67 positive tumor cells typically reside in hot spot regions. We stained and analyzed such hot spot regions from each TMA donor. The fraction of Ki-67 positive cells was significantly higher in sPGL as compared to PCCs (Fig. 1A, B; Table 2).

Since a large fraction of PPGLs presents with mutations affecting oxygen sensing, we stained our TMA for HIF-1α and HIF-2α. While 38% of HN-PGLs were positive, only 9% of PCCs and 0% of sPGLs expressed HIF-1α (Fig. 1C,D; Table 2). There was no difference in HIF-1α staining between non-metastatic and metastatic tumors (Supplementary Table S4).

Figure 2. *PPGLs express high levels of cytoplasmic HIF-2α and cytoplasmic HIF-2α is highly expressed in metastatic sPGLs.* (**A**) Representative images from tumor cores scored as negative (0), weak (1+), intermediate (2+) or strong (3+) for HIF-2α. (**B**) Quantification of positive cells for nuclear HIF-2α (HIF-2α-N) (in %). (**C**) H-score for cytoplasmic HIF-2α (HIF-2α-C). (**D**) Quantification of fraction (in %) of positive tumor cores for nuclear and cytoplasmic HIF-2α. (**E**) Quantification of fraction (in %) of tumor cores staining with high intensity (scored 2–3) for nuclear and cytoplasmic HIF-2α. (**F**)–(**G**) Expression of nuclear (HIF-2α-N) (F) and cytoplasmic (HIF-2α-C) (G) HIF-2α as divided by low (0–1) and high (2–3) staining intensity in sPGL, HN-PGL and PCC tumor subgroups. Tumor cores were scored manually by three independent researchers as well as semi-automatically using the QuPath-0.3.0 software. Statistical significance was determined by the Mann–Whitney test in B-C and Fisher's exact test in D-G. sPGL, sympathetic paraganglioma; HN-PGL, head- and neck paraganglioma; PCC, pheochromocytoma. The scale bar represents 100 µm in core images and 50 µm in zoomed images. Note that there are no metastatic HN-PGLs in this cohort.

HIF-2α expression is mainly cytoplasmic in all paragangliomas. HIF-2α positive tumor cores showed a high degree of cytoplasmic staining (Fig. 2A; Table 2), in concordance with findings in glioblastoma[29], neuroblastoma[28], and neural crest development[30]. We therefore decided to divide our analyses into nuclear and cytoplasmic HIF-2α. Evaluation of staining intensity of HIF-2α revealed that the majority of tumors scored negative for nuclear HIF-2α, while highly intense cytoplasmic HIF-2α staining was observed in 69% of sPGLs, 92% of HN-PGLs and 33% of PCCs (Fig. 2B–E; Table 2). To address HIF-2 activity in these tumors, we stained for HIF-2 specific target gene DEC1/BHLBE40, and found that the majority of tumors from all subtypes expressed this protein (Supplementary Table S3).

Metastatic sPGLs express high levels of cytoplasmic HIF-2α. We analyzed cytoplasmic HIF-2α in non-metastatic and metastatic PPGL patients based on their mutational status and observed that expression was not affected (Supplementary Table S4). When analyzing the sPGL cohort for cytoplasmic HIF-2α in non-metastatic and metastatic cases in depth, we observed that virtually all tumors from patients with metastasis expressed HIF-2α with high intensity (Supplementary Table S5). This was true for patients with SDHx mutations as well as without any known mutations (Supplementary Table S4), suggesting that staining for cytoplasmic HIF-2α may be useful to detect aggressive tumors that would otherwise have been missed using SDH screening immunohistochemistry.

Expression of nuclear HIF-2α was unchanged in non-metastatic vs. metastatic tumors in all three PPGL entities (Fig. 2F). In coherence with cytoplasmic HIF-2α staining at low intensity in PCCs overall, there was no difference in expression in non-metastatic as compared to metastatic tumors (Fig. 2G; Supplementary Table S5). Notably, while 57% of non-metastatic sPGLs strongly expressed cytoplasmic HIF-2α, this number increased to 83% in metastatic tumors (Fig. 2G; Supplementary Table S5).

Cytoplasmic HIF-2α correlates to proliferation proxy Ki-67. To determine the putative clinical impact of cytoplasmic HIF-2α, we investigated possible relationships with PPGL diagnostic markers. When investigating PPGLs as one entity, we found that cytoplasmic HIF-2α positively correlated with SYP, DEC1/BHLHE40 and Ki-67, while there was an inverse correlation with CgA expression (Fig. 3A,B). Correlation between HIF-2α and Ki-67 was strongest in sPGLs (Fig. 3C).

EPAS1 expression is higher in sPGLs. We analyzed expression of HIF-2α in five tumors with *EPAS1* mutations from two different cohorts (one tumor from TMA; four tumors from the CNIO study cohort[32]). All of these tumors (1 PCC and 4 sPGLs) expressed cytoplasmic HIF-2α (Supplementary Fig. S4 and Supplementary Table S6).

We have previously performed whole exome sequencing and expression microarray on a subset of PPGLs included in our TMA[33]. Here we utilized this material to analyze *HIF1A* and *EPAS1* expression in relation to mutation status and clinical features. Expression of *HIF1A* mRNA was slightly higher in the pseudohypoxic cluster, but half of the tumors in this group still displayed low levels (Fig. 3D). We could not detect any correlations between *HIF1A* mRNA and mutation status, metastasis, or diagnosis (Fig. 3D). Analysis of *EPAS1* expression showed substantially higher expression levels in tumors belonging to the pseudohypoxic cluster (Fig. 3D–E). We did not find a correlation between mRNA and cytoplasmic HIF-2α expression as most tumors in the kinase signaling cluster express the protein, but low mRNA levels (Fig. 3A,F).

We further investigated mRNA expression in correlation to tumor subtype and found that *EPAS1* levels were higher in sPGLs as compared to PCCs (Fig. 3G), in line with protein data (Fig. 2). We confirmed these findings in two independent cohorts (TCGA, n = 177 and Korpershoek, n = 49; Fig. 3H–I). While we could not assess *EPAS1* expression between PPGL subtypes in the Favier data set (n = 188) due to lack of such data, we detected higher mRNA levels in pseudohypoxic tumors as compared to all other groups (Fig. 3J).

High expression cytoplasmic HIF-2α predicts worse survival in sPGL patients. To investigate the survival status in our cohort, we used clinical follow-up data where 25 patients had died at an endpoint of 10 years (Supplementary Table S7). Dividing the cohort according to diagnosis, 15% of PCC, and as many as 46% of sPGL patients were deceased. Out of these 25 patients in total, 9 had died from cancer (5 from metastatic PPGL and 4 from other cancers), while the remaining 16 patients died of other causes (heart-related, infections, multi-organ failure, stroke, or other or unknown reasons). The survival probability did not differ between PCC and PGL patients when taking all causes of death into consideration (Fig. 4A). However, when further dividing

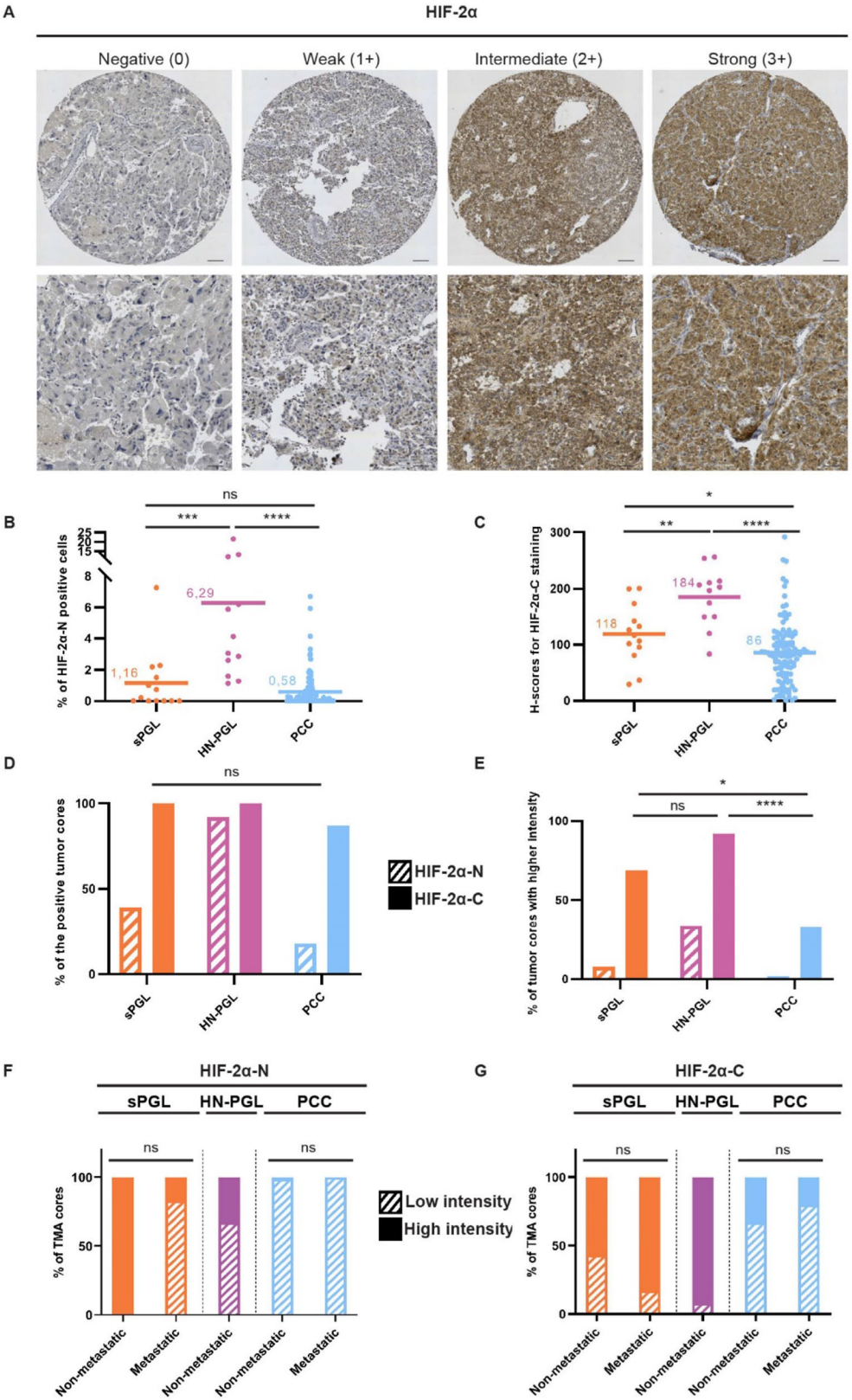
A
HIF-2α
Negative (0)
Weak (1+)
Intermediate (2+)
Strong (3+)
B
% of HIF-2α-N positive cells
1,16
6,29
0,58
sPGL
HN-PGL
PCC
C
H-scores for HIF-2α-C staining
118
184
86
D
% of the positive tumor cores
HIF-2α-N
HIF-2α-C
E
% of tumor cores with higher intensity
F
HIF-2α-N
G
HIF-2α-C
% of TMA cores
Low intensity
High intensity
Non-metastatic
Metastatic

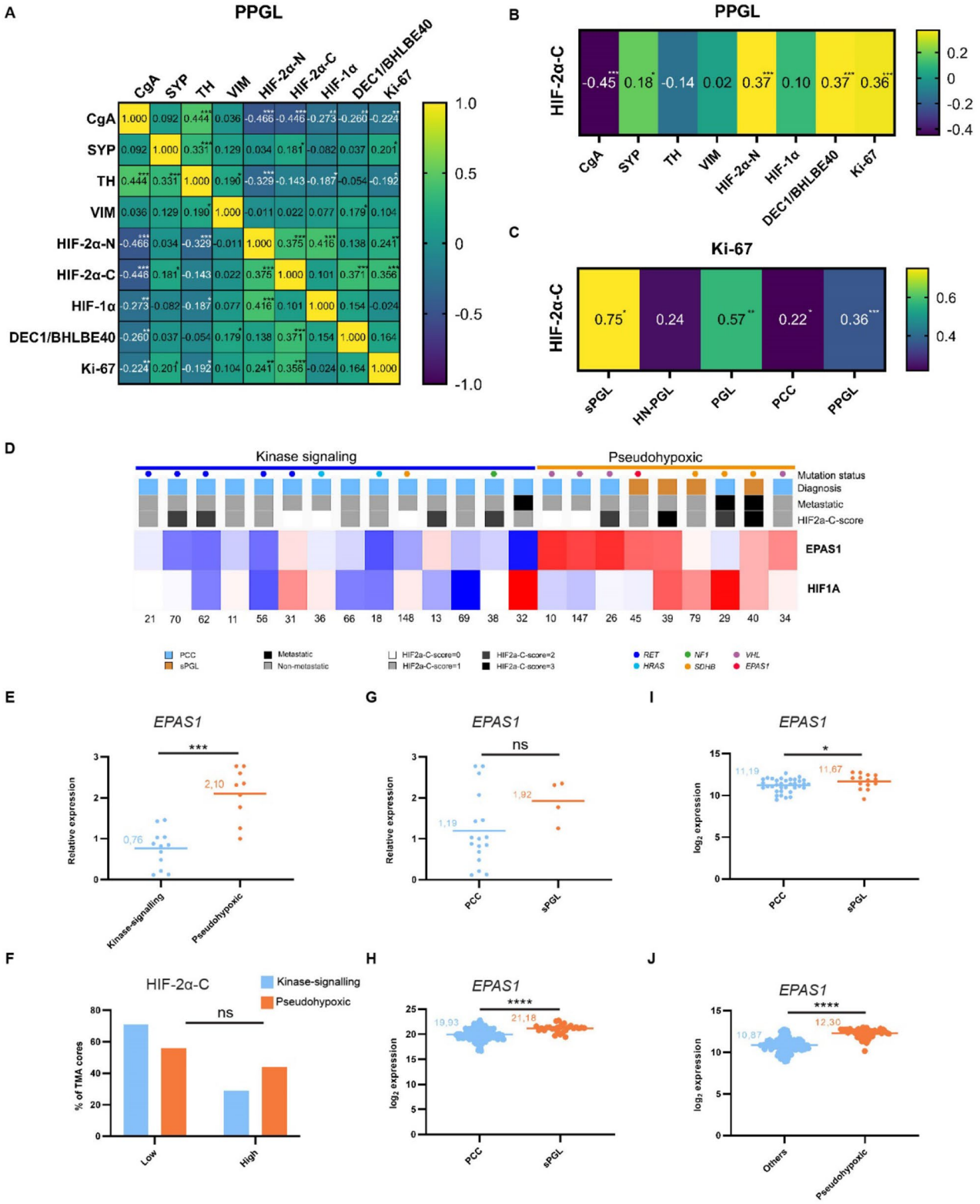
A
PPGL
CgA
SYP
TH
VIM
HIF-2α-N
HIF-2α-C
HIF-1α
DEC1/BHLBE40
Ki-67
1.0
0.5
0
-0.5
-1.0
B
PPGL
HIF-2α-C
0.2
0
-0.2
-0.4
C
Ki-67
HIF-2α-C
0.6
0.4
sPGL
HN-PGL
PGL
PCC
PPGL
D
Kinase signaling
Pseudohypoxic
Mutation status
Diagnosis
Metastatic
HIF2a-C-score
EPAS1
HIF1A
21 70 62 11 56 31 36 66 18 148 13 69 38 32 10 147 26 45 39 79 29 40 34
PCC
sPGL
Metastatic
Non-metastatic
HIF2a-C-score=0
HIF2a-C-score=1
HIF2a-C-score=2
HIF2a-C-score=3
RET
HRAS
NF1
SDHB
VHL
EPAS1
E
EPAS1
***
Relative expression
0,76
2,10
Kinase-signalling
Pseudohypoxic
G
EPAS1
ns
Relative expression
1,19
1,92
PCC
sPGL
I
EPAS1
*
log2 expression
11,19
11,67
PCC
sPGL
F
HIF-2α-C
Kinase-signalling
Pseudohypoxic
ns
% of TMA cores
Low
High
H
EPAS1
****
log2 expression
19,93
21,18
PCC
sPGL
J
EPAS1
****
log2 expression
10,87
12,30
Others
Pseudohypoxic

◂**Figure 3.** *Cytoplasmic HIF-2α correlates to proliferation in sPGLs and EPAS1 mRNA expression is higher in sPGL as compared to PCC.* (**A**) Compilation of correlations between all markers stained for in this cohort. (**B**) Compilation of correlations only between cytoplasmic HIF-2α and the other markers for visualization. (**C**) Correlations between cytoplasmic HIF-2α and Ki-67 as divided into the different subgroups of PPGL. (**D**) *HIF1A* and *EPAS1* mRNA expression in a subset of tumors from our TMA cohort, analyzed by whole exome sequencing. (**E**) Expression of *EPAS1* mRNA in the pseudohypoxic and kinase-signaling groups from (D). (**F**) Quantification of fraction of TMA cores scored as low or high for cytoplasmic HIF-2α in the pseudohypoxic and kinase-signaling groups. (**G**)–(**I**). Expression of *EPAS1* mRNA as determined by RNA sequencing in sPGLs and PCCs in three different cohorts; TMA (n = 21, G), TCGA (n = 177, H) and Korpershoek (n = 49, I). (**J**) Expression of *EPAS1* mRNA as determined by RNA sequencing in pseudohypoxic as compared to all other subgroups in the Favier cohort (n = 188). Correlation coefficient was calculated using Spearman's correlation test in GraphPad Prism 9 and statistical significance (two-tailed P value for each correlation coefficient) was computed automatically by the software. Statistical significance was determined using Mann–Whitney test in E, G-J and Fisher's exact test in F. PCC, pheochromocytoma; sPGL, sympathetic paraganglioma.

into PGL subtypes, sPGLs displayed a significantly worse prognosis than PCCs and HN-PGLs (Fig. 4B). Since it is difficult to determine whether the cause of death from other reasons than metastatic PPGLs were due to their primary tumor, we stratified survival probability only in patients that died from metastatic disease. There was no pronounced difference when comparing PCC and PGL (Fig. 4C). Although few patients in this cohort died from their disease, when further stratifying PGL patients, there is a separation where sPGL patients have worse prognosis (survival rate only 68% for sPGL, while 100% for HN-PGL and 98% for PCC) (Fig. 4D).

While there was no correlation between cytoplasmic HIF-2α and outcome in PPGL or PCC entities (Fig. 4E,F), high intensity of cytoplasmic HIF-2α predicts poor outcome in PGL patients (Fig. 4G), with a more pronounced effect in sPGL patients specifically (Fig. 4H).

Discussion

There is a lack of accessible material for biological analyses of PPGL. We present a TMA of cores from 149 individual patients with PCCs, HN-PGLs and sPGLs, reflecting patient distribution of all clinical parameters. We demonstrate that this material is valuable by extensive characterization of protein markers used in diagnostics in connection to primary tumor location, non-metastatic vs. metastatic disease, mutation status, biochemical phenotype, and importantly 10-year follow-up data. In addition, we add RNA expression data from a selection of these patients.

Half of sPGL patients in our cohort present with metastatic disease, and in coherence, patients from this tumor entity have a worse prognosis and lower survival rate as compared to PCC and HN-PGL. This strengthens the benefit of the WHO classification of these three subgroups for diagnostics, when assessing treatment regimens and patient follow-up schemes. It has recently been further demonstrated that metastatic HN-PGLs have a longer disease-specific survival than metastatic PPGLs, and that extra-adrenal PPGLs (*i.e.,* PGL as compared to PCC) have a worse prognosis[41], in line with our data.

PPGLs within the pseudohypoxic group present with a more aggressive behavior and worse prognosis. Mutations in the *EPAS1* gene confer such a pseudohypoxic profile and represent a subgroup of its own within the pseudohypoxic group of tumors[24]. We have, in previous studies on neural crest cells during embryogenesis as well as in neuroblastoma, observed that the HIF-2α protein non-canonically localizes to the cytoplasm[28,30]. There was a clear distinction between the percentage of tumors positive for cytoplasmic vs. nuclear protein in PPGLs, and considering their proposed shared ancestor cells, the neural crest, with neuroblastoma (shown in e.g., composite tumors[42]), these findings are of importance to further understand PPGL initiation and subtype distinction.

The relatively high expression of HIF-1α and nuclear and cytoplasmic HIF-2α in HN-PGLs is explained by the fact that these tumors are located in the oxygen sensing carotid body. In contrast, sPGLs express no or very low levels of HIF-1α and nuclear HIF-2α, while all of them express substantial levels of cytoplasmic HIF-2α. This suggests that the presence of cytoplasmic HIF-2α in sPGLs is not due to a hypoxic environment in these tumors, but rather present with a bona fide pseudohypoxic phenotype mediated via non-canonical mechanisms for regulation of HIF-2α and downstream activity.

PPGLs are to a large extent slow growing, and the assessment of Ki-67 expression as a proxy for proliferation in clinical assessment of these tumors is of significant value for prognostics. Sympathetic PGLs display substantially higher expression of Ki-67 and in coherence with this more proliferative phenotype predicts poor outcome for patients that die from their primary tumor. Cytoplasmic HIF-2α correlates positively to Ki-67, and is highly and intensely expressed in the majority of metastatic sPGLs cases. While all sPGL patients that present with low tumor intensity of cytoplasmic HIF-2α survive, the fraction of patients with high intensity-expressing tumors presents with a survival probability of 68%. It is however important to note that the number of patients that die from their primary or metastatic tumor is low, and additional studies with other cohorts should be performed.

The mechanism-of-action for cytoplasmic HIF-2α is yet unknown, and ongoing functional studies aim to assess its direct role in PPGL subtype initiation and progression. Our data show that *EPAS1* mRNA expression is substantially increased in the pseudohypoxic- as compared to the kinase PPGL subgroup. However, both groups express high cytoplasmic HIF-2α, suggesting that HIF-2α is regulated at a (post-)translational-rather than transcriptional level.

To assess the role of HIF-2α in PPGL progression, Bechmann and colleagues knocked down or overexpressed HIF-2α in cell line models, and showed that HIF-2α induced a pro-metastatic phenotype[43]. The HIF-2α-driven effects on the PPGL cells were due to protein function per se and not hypoxia-induced mechanisms[43]. These

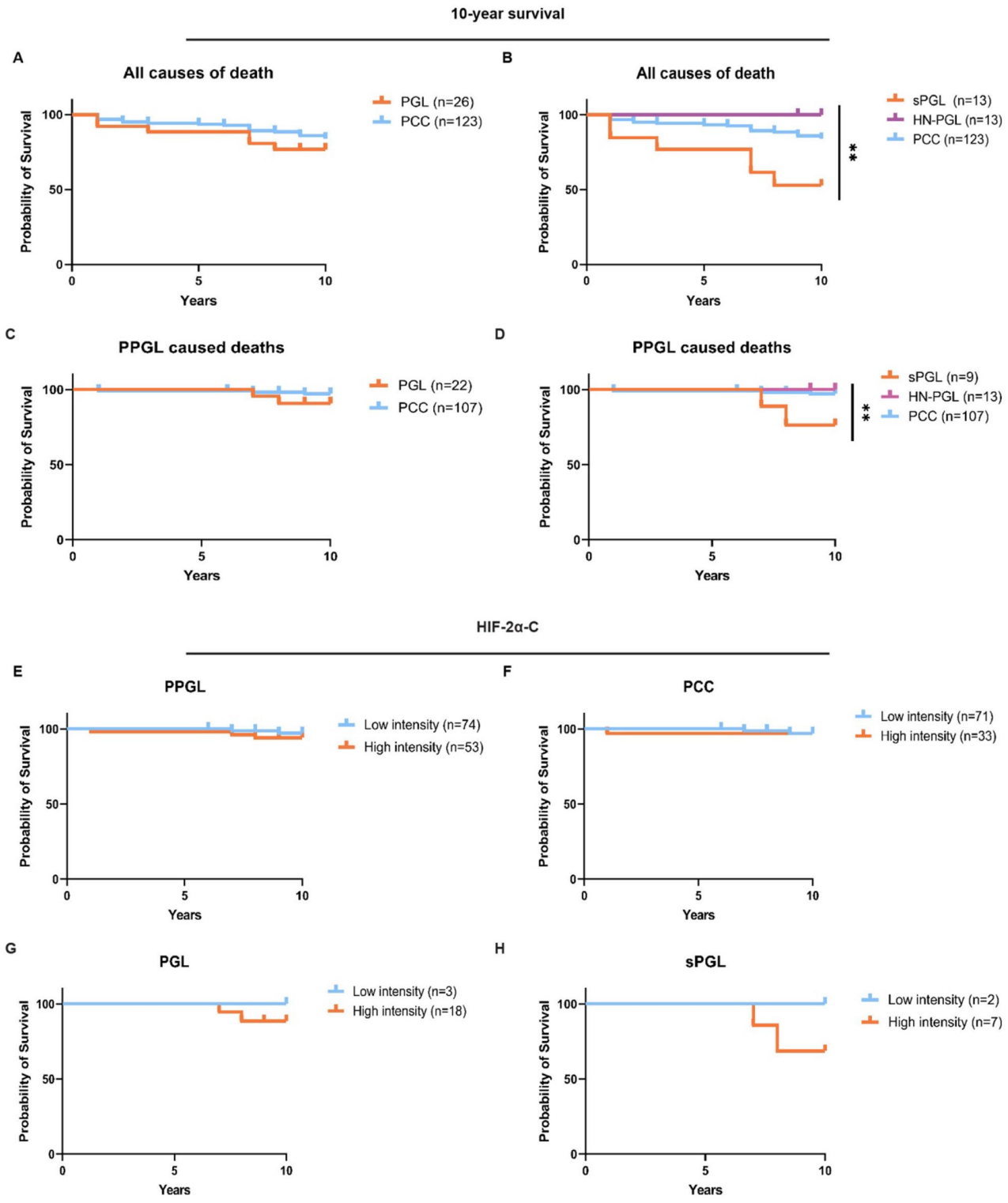

Figure 4. *Intense staining of cytoplasmic HIF-2α predicts poor outcome in sPGLs.* (**A**) Survival probability (10-year follow-up) of PPGL patients when including all causes of death. (**B**) Survival probability (10-year follow-up) of patients when only including patients dead from PPGL disease comparing PCC and PGL subgroups. (**C**)–(**D**) Survival probability (10-year follow-up) of PPGL patients divided into PGL and PCC subgroups when including all causes of death (C) and only PPGL caused deaths (D). (**E**)–(**F**) Survival probability stratified by low (0–1) and high (2–3) staining intensity of cytoplasmic HIF-2α in the entire PPGL cohort (**E**) and PCC (**F**). (**G**)–(**H**) Survival probability (10-year follow-up) of patients when only including patients dead from PPGL disease in PGL (**G**) and sPGL (**H**) comparing low (0–1) and high (2–3) staining intensity of cytoplasmic HIF-2α. Statistical significance was calculated using the Log-rank (Mantel–Cox) test. *PCC* pheochromocytoma, *sPGL* sympathetic paraganglioma, *HN-PGL* head- and neck paraganglioma, *PGL* paraganglioma, *PPGL* pheochromocytoma and paraganglioma.

data on overall HIF-2α protein expression in PPGL as one tumor entity, in combination with our results on the dependence of cytoplasmic HIF-2α in the different tumor subtypes, suggest an important tumor-driving role of HIF-2α in these tumors. sPGLs and neuroblastomas arise along the sympathetic chain ganglia and share a common ancestor cell in the trunk neural crest. It is therefore of particular interest that the HIF-2α protein is expressed in oxygenated cells, is mainly cytoplasmic, and that this fraction of cells predicts poor outcome in both of these tumor types. In addition, the high expression of cytoplasmic HIF-2α in metastatic sPGLs is coherent with the correlation between intensely HIF-2α positive tumor cells and distal metastasis in neuroblastoma. Since sPGL patients present with significantly worse survival than PCC and HN-PGL patients, routinely assessing HIF-2α expression in sPGL could represent a new diagnostic biomarker and aid in treatment decisions and patient follow-up.

Data availability

The data underlying this article will be shared on reasonable request to the corresponding author.

Received: 20 March 2023; Accepted: 11 July 2023
Published online: 18 July 2023

References

1. Furlan, A. *et al.* Multipotent peripheral glial cells generate neuroendocrine cells of the adrenal medulla. *Science* **357**, 6346. https://doi.org/10.1126/science.aal3753 (2017).
2. Kameneva, P. *et al.* Single-cell transcriptomics of human embryos identifies multiple sympathoblast lineages with potential implications for neuroblastoma origin. *Nat. Genet.* **53**(5), 694–706. https://doi.org/10.1038/s41588-021-00818-x (2021).
3. Ayala-Ramirez M. *et al.* Clinical Risk Factors for Malignancy and Overall Survival in Patients with Pheochromocytomas and Sympathetic Paragangliomas: Primary Tumor Size and Primary Tumor Location as Prognostic Indicators. *J. Clin. Endocrinol. Metab.* **96**(3), 717–725. https://doi.org/10.1210/jc.2010-1946 (2011).
4. Lam, A. K. Update on adrenal tumours in 2017 World Health Organization (WHO) of Endocrine Tumours. *Endocr. Pathol.* **28**(3), 213–227. https://doi.org/10.1007/s12022-017-9484-5 (2017).
5. Dahia, P. L. M. Pheochromocytoma and paraganglioma pathogenesis: learning from genetic heterogeneity. *Nat. Rev. Cancer* **14**(2), 108–119. https://doi.org/10.1038/nrc3648 (2014).
6. Fishbein, L. *et al.* Whole-exome sequencing identifies somatic ATRX mutations in pheochromocytomas and paragangliomas. *Nat. Commun.* **6**(1), 6140. https://doi.org/10.1038/ncomms7140 (2015).
7. Fishbein, L. *et al.* Comprehensive molecular characterization of pheochromocytoma and paraganglioma. *Cancer Cell* **31**(2), 181–193. https://doi.org/10.1016/j.ccell.2017.01.001 (2017).
8. Dwight, T. *et al.* Functional significance of germline EPAS1 variants. *Endocr. Relat. Cancer* **28**(2), 97–109. https://doi.org/10.1530/ERC-20-0280 (2021).
9. Wachtel, H. & Fishbein, L. Genetics of pheochromocytoma and paraganglioma. *Curr. Opin. Endocrinol. Diabetes Obes.* **28**(3), 283–290. https://doi.org/10.1097/MED.0000000000000634 (2021).
10. Wilzén, A. *et al.* Malignant pheochromocytomas/paragangliomas harbor mutations in transport and cell adhesion genes: Sequencing of pheochromocytoma/paraganglioma. *Int. J. Cancer* **138**(9), 2201–2211. https://doi.org/10.1002/ijc.29957 (2016).
11. López-Jiménez, E. *et al.* Research resource: Transcriptional profiling reveals different pseudohypoxic signatures in SDHB and VHL-related pheochromocytomas. *Mol. Endocrinol.* **24**(12), 2382–2391. https://doi.org/10.1210/me.2010-0256 (2010).
12. Dahia, P. L. M. *et al.* A HIF1α Regulatory Loop Links Hypoxia and Mitochondrial Signals in Pheochromocytomas. *PLoS Genet.* **1**(1), e8. https://doi.org/10.1371/journal.pgen.0010008 (2005).
13. Burnichon, N. *et al.* Integrative genomic analysis reveals somatic mutations in pheochromocytoma and paraganglioma. *Hum. Mol. Genet.* **20**(20), 3974–3985. https://doi.org/10.1093/hmg/ddr324 (2011).
14. Hammarlund, U. E., Flashman, E., Mohlin, S. & Licausi, F. Oxygen-sensing mechanisms across eukaryotic kingdoms and their roles in complex multicellularity. *Science* **370**(6515), eaba3512. https://doi.org/10.1126/science.aba3512 (2020).
15. Choueiri, T. K. & Kaelin, W. G. Targeting the HIF2–VEGF axis in renal cell carcinoma. *Nat. Med.* **26**(10), 1519–1530. https://doi.org/10.1038/s41591-020-1093-z (2020).
16. Zhuang, Z. *et al.* Somatic *HIF2A* gain-of-function mutations in paraganglioma with polycythemia. *N. Engl. J. Med.* **367**(10), 922–930. https://doi.org/10.1056/NEJMoa1205119 (2012).
17. Favier, J., Buffet, A. & Gimenez-Roqueplo, A. HIF2A mutations in Paraganglioma with polycythemia. *N Engl J Med.* **367**(22), 2161–2162. https://doi.org/10.1056/NEJMc1211953 (2012).
18. Comino-Méndez, I. *et al.* Tumoral EPAS1 (HIF2A) mutations explain sporadic pheochromocytoma and paraganglioma in the absence of erythrocytosis. *Hum. Mol. Genet.* **22**(11), 2169–2176. https://doi.org/10.1093/hmg/ddt069 (2013).
19. Lorenzo, F. R. *et al.* A novel EPAS1/HIF2A germline mutation in a congenital polycythemia with paraganglioma. *J. Mol. Med.* **91**(4), 507–512. https://doi.org/10.1007/s00109-012-0967-z (2013).
20. Pacak, K. *et al.* New syndrome of paraganglioma and somatostatinoma associated with polycythemia. *J. Clin. Oncol.* **31**(13), 1690–1698. https://doi.org/10.1200/JCO.2012.47.1912 (2013).
21. Toledo, R. A. *et al.* In vivo and in vitro oncogenic effects of HIF2A mutations in pheochromocytomas and paragangliomas. *Endocr. Relat. Cancer* **20**(3), 349–359. https://doi.org/10.1530/ERC-13-0101 (2013).
22. Welander, J. *et al.* Frequent EPAS1/HIF2α exons 9 and 12 mutations in non-familial pheochromocytoma. *Endocr. Relat. Cancer* **21**(3), 495–504. https://doi.org/10.1530/ERC-13-0384 (2014).
23. Islam, F., Pillai, S., Gopalan, V. & Lam, A.K.-Y. Identification of novel mutations and expressions of EPAS1 in phaeochromocytomas and paragangliomas. *Genes* **11**(11), 1254. https://doi.org/10.3390/genes11111254 (2020).
24. Fliedner, S. M. J. *et al.* Hypoxia-inducible factor 2α mutation-related paragangliomas classify as discrete pseudohypoxic subcluster. *Neoplasia* **18**(9), 567–576. https://doi.org/10.1016/j.neo.2016.07.008 (2016).
25. Islam, F., Gopalan, V., Law, S., Lam, A. K. & Pillai, S. Molecular deregulation of EPAS1 in the pathogenesis of esophageal squamous cell carcinoma. *Front. Oncol.* **10**, 1534. https://doi.org/10.3389/fonc.2020.01534 (2020).
26. Islam, F., Gopalan, V., Lu, C. T., Pillai, S. & Lam, A. K. Identification of novel mutations and functional impacts of EPAS1 in colorectal cancer. *Cancer Med.* **10**(16), 5557–5573. https://doi.org/10.1002/cam4.4116 (2021).
27. Holmquist-Mengelbier, L. *et al.* Recruitment of HIF-1α and HIF-2α to common target genes is differentially regulated in neuroblastoma: HIF-2α promotes an aggressive phenotype. *Cancer Cell* **10**(5), 413–423. https://doi.org/10.1016/j.ccr.2006.08.026 (2006).
28. Persson, C. U. *et al.* ARNT-dependent HIF-2 transcriptional activity is not sufficient to regulate downstream target genes in neuroblastoma. *Exp. Cell Res.* **388**(2), 111845. https://doi.org/10.1016/j.yexcr.2020.111845 (2020).
29. Li, Z. *et al.* Hypoxia-inducible factors regulate tumorigenic capacity of glioma stem cells. *Cancer Cell* **15**(6), 501–513. https://doi.org/10.1016/j.ccr.2009.03.018 (2009).

30. Niklasson, C. U. *et al.* Hypoxia inducible factor-2α importance for migration, proliferation, and self-renewal of trunk neural crest cells. *Dev. Dyn.* **250**(2), 191–236. https://doi.org/10.1002/dvdy.253 (2021).
31. Bankhead, P. *et al.* QuPath: Open source software for digital pathology image analysis. *Sci. Rep.* **7**(1), 16878. https://doi.org/10.1038/s41598-017-17204-5 (2017).
32. Monteagudo, M. *et al.* Analysis of telomere maintenance related genes reveals NOP10 as a new metastatic-risk marker in pheochromocytoma/paraganglioma. *Cancers* **13**(19), 4758. https://doi.org/10.3390/cancers13194758 (2021).
33. Tomić, T. T. *et al.* MYO5B mutations in pheochromocytoma/paraganglioma promote cancer progression. *PLOS Genet.* **16**(6), 1008803. https://doi.org/10.1371/journal.pgen.1008803 (2020).
34. Richards, S. *et al.* Standards and guidelines for the interpretation of sequence variants: a joint consensus recommendation of the American College of Medical Genetics and Genomics and the Association for Molecular Pathology. *Genet. Med.* **17**(5), 405–424. https://doi.org/10.1038/gim.2015.30 (2015).
35. Loriot, C. *et al.* Epithelial to mesenchymal transition is activated in metastatic pheochromocytomas and paragangliomas caused by SDHB gene mutations. *J. Clin. Endocrinol. Metab.* **97**(6), 954–962. https://doi.org/10.1210/jc.2011-3437 (2012).
36. Evenepoel, L. *et al.* Expression of contactin 4 is associated with malignant behavior in pheochromocytomas and paragangliomas. *J. Clin. Endocrinol. Metab.* **103**(1), 46–55. https://doi.org/10.1210/jc.2017-01314 (2018).
37. Muth, A. *et al.* Prevalence of germline mutations in patients with pheochromocytoma or abdominal paraganglioma and sporadic presentation: A population-based study in Western Sweden. *World J. Surg.* **36**(6), 1389–1394. https://doi.org/10.1007/s00268-012-1430-6 (2012).
38. Rana, M. U. *et al.* Head and neck paragangliomas in Norway importance of genetics updated diagnostic workup and treatment. *Acta Oto-Laryngologica* **141**(3) 303–308. https://doi.org/10.1080/00016489.2020.1845397 (2021).
39. Maher, E. R. The pressure rises: Update on the genetics of phaeochromocytoma. *Hum. Mol. Genet.* **11**(20), 2347–2354. https://doi.org/10.1093/hmg/11.20.2347 (2002).
40. Pasini, B. & Stratakis, C. A. SDH mutations in tumorigenesis and inherited endocrine tumours: Lesson from the phaeochromocytoma-paraganglioma syndromes. *J. Intern. Med.* **266**(1), 19–42. https://doi.org/10.1111/j.1365-2796.2009.02111.x (2009).
41. Pamporaki, C. *et al.* Determinants of disease-specific survival in patients with and without metastatic pheochromocytoma and paraganglioma. *Eur. J. Cancer* **169**, 32–41. https://doi.org/10.1016/j.ejca.2022.03.032 (2022).
42. Tasaka, K. *et al.* Oncogenic *FGFR1* mutation and amplification in common cellular origin in a composite tumor with neuroblastoma and pheochromocytoma. *Cancer Sci.* **113**(4), 1535–1541. https://doi.org/10.1111/cas.15260 (2022).
43. Bechmann, N. *et al.* HIF2α supports pro-metastatic behavior in pheochromocytomas/paragangliomas. *Endocr. Relat. Cancer* **27**(11), 625–640. https://doi.org/10.1530/ERC-20-0205 (2020).

Acknowledgements

The authors would like to thank Siv Beckman, Christina Möller, Gülay Altiparmak, and Yvonne Arvidsson for excellent technical assistance and Dr. Hans K. Ghayee for kindly providing hPheo1 cells.

Author contributions

Conceptualization: S.K., L.G., E.E., B.W., F.A., S.P., A.M., S.M.; Data curation: S.K., L.G., F.A.; Formal analysis: S.K., L.G.; Investigation: S.K., L.G., F.A., O.N., S.P.; Methodology: S.K., L.G., F.A., S.P., A.M., S.M.; Resources: M.R., O.N., B.W., F.A., A.M.; Validation: S.K., L.G., F.A., S.P.; Visualization: S.K., F.A.; Writing—original draft: S.M.; Writing—review & editing: S.K., L.G., E.E., P.M.S., M.R., O.N., B.W., F.A., S.P., A.M., S.M.; Supervision: A.M., S.M.; Project administration: A.M., S.M.; Funding acquisition: B.W., A.M., S.M.

Funding

Open access funding provided by Lund University. This work was supported by The Mrs Berta von Kamprad's Foundation; the Swedish Cancer Society; the Swedish Childhood Cancer Fund; the Lions Cancer Fund West; and institutional research funds at the Department of Surgery, Sahlgrenska University Hospital.

Competing interests

The authors declare no competing interests.

Additional information

Supplementary Information The online version contains supplementary material available at https://doi.org/10.1038/s41598-023-38606-8.

Correspondence and requests for materials should be addressed to S.M.

Reprints and permissions information is available at www.nature.com/reprints.

Publisher's note Springer Nature remains neutral with regard to jurisdictional claims in published maps and institutional affiliations.